UC Irvine
UC Irvine Previously Published Works

Title

A novel transillumination meibography device for in vivo imaging of mouse meibomian glands.

Permalink

https://escholarship.org/uc/item/9b18t4tv

Authors

Hwang, Ho

Mikula, Eric

Xie, Yilu

et al.

Publication Date

2021

DOI

10.1016/j.jtos.2020.08.012

Peer reviewed

eScholarship.org Powered by the California Digital Library
University of California

Author Manuscript

Author Manuscript

Author Manuscript

Author Manuscript

HHS Public Access

Author manuscript

Ocul Surf. Author manuscript; available in PMC 2023 July 31.

Published in final edited form as:

Ocul Surf. 2021 January ; 19: 201–209. doi:10.1016/j.jtos.2020.08.012.

A novel transillumination meibography device for *in vivo* imaging of mouse meibomian glands

Ho Sik Hwang[a,b], **Eric Mikula**[b], **Yilu Xie**[b], **Donald J. Brown**[b], **James V. Jester**[b,*]

[a]Department of Ophthalmology, College of Medicine, The Catholic University of Korea, Seoul, Republic of Korea

[b]Department of Ophthalmology, University of California, Irvine, Irvine, CA, United States

Abstract

Purpose: While mouse models of dry eye disease (DED) have been developed, studies evaluating the role of the meibomian glands limited by the inability to temporally document changes. In this report we describe the development of a novel mouse transillumination meibography device and assess the ability of this device to detect age-related changes in the meibomian glands of young and old mice.

Methods: The mouse meibography device was comprised of a 3 mm wide right angle prism attached to broad spectrum light source by an optical fiber. Eyelids were then pulled over the prism using double tooth forceps and imaged using a stereomicroscope and low light level camera. Meibomian glands from four young and four old male, BALB/c mice were then imaged and analyzed using ImageJ.

Results: In young mice, meibography documented the presence of 7–8 meibomian glands appearing as black and distinct eyelid structures with the length shorter in the lower eyelid compared to the upper eyelids. Eyelids of old mice showed apparent dropout of meibomian glands along with smaller and more irregularly shaped acini. The mean acini area of one meibomian gland was 0.088 ± 0.025 mm^2 in young mice and 0.080 ± 0.020 mm^2 in old mice ($p = 0.564$), but the Meibomian gland density was significantly lower in older mice (41.7 ± 6.4%, 27.3 ± 4.2%) ($p = 0.021$).

Conclusion: We have developed an *in vivo* meibography device that may prove useful in sequentially documenting changes during development of meibomian gland dysfunction and following treatment.

Keywords

Meibomian gland; Meibography; Age-related meibomian gland dysfunction

*Corresponding author. 843 Health Sciences Road, University of California, Irvine, Irvine, CA, 92697, United States. JJester@uci.edu (J.V. Jester).

Appendix A. Supplementary data

Supplementary data related to this article can be found at https://doi.org/10.1016/j.jtos.2020.08.012.

Author Manuscript Author Manuscript Author Manuscript Author Manuscript

Introduction

Dry eye disease (DED) is a common ocular surface disorder that is currently classified into an aqueous deficient (ADDED) and/or evaporative (EDED) type [1]. While the lacrimal gland plays an important role in the development of ADDED, EDED is thought to involve meibomian gland dysfunction (MGD) leading to decreased or abnormal lipid secretion onto the tear film causing increased tear evaporation, tear hyper osmolarity and ocular surface inflammation [2]. Meibomian glands are lipid synthesizing, modified sebaceous glands embedded in the eyelid tarsal plate that secrete oil (meibum) onto to the tear film [3].

Like other diseases, animal models have the potential to provide insights into the cellular and molecular mechanisms underlying the development of DED and the role that the meibomian glands play in the pathogenesis of this disorder. Towards this end, mouse models have established that environmental stress in the form of a low humidity environment can lead to ocular surface inflammation and the development of DED signs including decrease tears and increased corneal surface fluorescein staining [7–11]. Additionally, changes in the meibomian gland following exposure to dry environments has also been noted [12], but the correlation between meibomian gland changes in ocular surface inflammation have yet to be clearly identified Besides environmental stress, transgenic mice showing abnormal growth and/or development of the meibomian glands have also been identified [13], but the correlation between gland and ocular surface changes have been difficult to identify given the lack of methods available for documenting changes in the meibomian glands.

Currently, there are two main approaches to evaluating the morphological changes in the meibomian glands of mice. The first method uses a histologic approach requiring tissue fixation, processing and serial sectioning to identify key regions of the meibomian gland (central duct, gland orifice and acini) that are thought to be key targets for MGD [14,15]. Histologic analysis is highly subject to artifact, and selective sampling of the meibomian gland unless one performs serial sectioning with 3 dimensional reconstruction [16]. Alternatively, removal of both eyelids combined with en bloc staining and ex vivo biomicroscopy has been used to measure gland volume [17–20]. This approach has the advantage of higher reproducibility, but also suffers from the need to sacrifice the mice.

Over the years, transillumination meibography and reflectance meiboscopy have been used to evaluate changes in the meibomian gland of DED patients with MGD [21–28]. Meibography/meiboscopy is also easily performed on rabbits as shown recently by Eom et al. and others [21,29]. Meibography is a simple biomicroscopy technique that only requires transillumination of the eyelid and photography using a standard slit-lamp [22]. Furthermore, this imaging can be performed on live animals with anesthesia to document progressive changes in the gland. However, to our knowledge meibography has not been previously used to study meibomian gland function in the mouse. In this paper we describe a custom-made transilluminator that can be used to perform *in vivo* transillumination meibography of the mouse eyelid.

Author Manuscript Author Manuscript Author Manuscript Author Manuscript

Materials and methods

Animals

Eight male, BALB/c mice were used in this study, 4 young (<3 months old; #1–4) and 4 old (>15 months old; 4 male (#5–8)). Care and handling of mice conformed with the ARVO protocol for animal experiments and the consent of the University of California Irvine IACUC. Prior to eyelid photography, mice were anesthetized with inhalation anesthesia using 5% isoflurane mixed with 500 ml/min oxygen in an induction chamber. Mice were then transferred to a mouse holder under the dissecting microscope objective lens (Fig. 1) and anesthesia was maintained using a customized inhalation mask (isoflurane 1.5–2.0%, 100 ml/min oxygen) fabricated using a 1 ml Eppendorf pipette tip connected to the anesthetic coaxial gas tube (Kent Scientific, Torrington, CT) (Fig. 2). During the anesthesia, the mask was tightly attached to the nose and mouth of the mouse, and the gas tube connected to the mask was fixed with clay. Only the right eyelids (upper and lower) were photographed in all mice.

Dissection microscope with monochromatic camera

A binocular dissection microscope (Leica MZ16FA, Leica Microsystems, Heerbrugg, Switzerland) equipped with a monochromatic camera (DFC340FX, Leica Microsystems, Heerbrugg, Switzerland) was used to take biomicroscopic photographs of the right eyes of each mouse. The camera has no infrared (IR) blocking filter and no IR transmitting filter was used for this experiment. All images were taken at 28.3× magnification, the maximum magnification at which most of the meibomian glands of the eyelids could be observed.

Mouse holder

Because the mouse position is very important for good meibography, we used a mouse holder made with clay. The mouse was positioned so that the eyelids to be examined were located on the lower side. For example, when the meibomian glands in the upper lid were photographed, the mouse was placed in a supine position with the head adjusted so that the upper eyelid margin was horizontal (Fig. 3A), and the palpebral conjunctival plane was parallel to the objective lens of the dissecting microscope. For the lower eyelid, the mouse is placed in a prone position (Fig. 3B). In either the supine or prone position, the clay was deformed to fit the body and head of the mouse, then dried and used as a mouse holder in the following experiments.

Optical fiber and light probe

A broad band, halogen light source (OSL2 and OSL2B, Thorlabs, Newton, NJ) was used for the transillumination meibography. The light was delivered by a special optical fiber (BFL200HS02, Thorlabs, Newton, NJ) that had an input connector comprised of a bundle of seven 200 μm-diameter fibers and an output connector comprised of a linear array of fibers as shown in Fig. 4A. The linear array, output connector was then attached to a diffuser and a prism with glue. The diffuser was made of opaque, white plastic, 3 mm × 3 mm × 1 mm thickness. At the opposite end of the diffuser, a right-angle prism (PS605, Thorlabs, Newton, NJ) (3 mm) was attached (Fig. 4B) that reflected the light 90° to pass through the

Author Manuscript Author Manuscript Author Manuscript Author Manuscript

meibomian glands vertically. In addition, when the eyelid margin was held with forceps, the prism served to support the eyelid at the back (Fig. 4C).

Forceps

Polack forceps (8–0814T, Rumex, Clearwater, FL) was used to evert the eyelids (Fig. 5A). Polack forceps are special type of forceps used in cornea transplantation surgery. They have two pairs of teeth that can symmetrically hold the edges of a corneal button during corneal suturing. When the lid margin of mouse was held with these forceps and everted, the eyelid was flat and was not distorted to a triangular shape (Fig. 5B). The Polack forceps used in this study has two pairs of teeth with 1.5 mm separation.

Taking photographs

First, at a low magnification, the position of the mouse was adjusted so that the eyelid to be examined was located at the center of the field of view. The magnification was then increased to 28.3X, maintaining focus on the lid margin. Using the Polack forceps the middle edge of the eyelid margin was grasped, and eyelid pulled over the prism to evert the eyelid (Fig. 6). The meibomian glands were then brought into focus by adjusting the height of the light probe and the forceps holding the eyelid. Image exposure was adjusted to 10–20 ms, with a gamma value set at 1.5. A series of images were then collected as a video, and single images were saved at a resolution of 1600 × 1200 pixels.

Quantitative analysis

Since photographs of the temporal and nasal meibomian glands were generally not in focus, only the central, five meibomian glands were quantitatively analyzed by measuring the meibomian gland width, length and acinar diameter of the four young and four old mice (total 20 meibomian glands for each group). The width of a Meibomian gland was defined as the largest width of it. Furthermore, quantitative analysis of dropout was limited to the lower eyelid of each mouse due to the fact that it was difficult to clearly identify individual meibomian glands in the upper lid.

For each image, each Meibomian gland was then selected (Fig. 7A and B) using image J (version 1.38x; Wayne Rasband National Institutes of Health, Bethesda, MD) and the image threshold was adjusted so that only the acini were selected (Fig. 7C). The area occupied by the acini was then recorded. Acinar area was measured for each of five meibomian glands (MG_1, MG_2, MG_3, MG_4, MG_5), as well as the total acinar areas for the five meibomian glands ($MG = MG_1+MG_2+MG_3+MG_4+MG_5$) and mean acini area of a meibomian gland (MG/5). For each image, a region of interest (ROI) was defined by outlining five meibomian glands like Fig. 7D (from eyelid margin to distal end of Meibomian glands). The area of the region of interest covering the five meibomian glands (ROIA) was then measured and the Meibomian gland density was calculated 100% * total acinar area of five meibomian glands (MG)/total area of region of interest covering the five meibomian area (ROIA).

Assessment of reproducibility

To evaluate the reproducibility of transillumination meibography, the right lower eyelids of four young male mice (#1–4) and four old male mice (#5–8) were photographed for two

Author Manuscript Author Manuscript Author Manuscript Author Manuscript

consecutive days. The acini area of five meibomian glands in the center were measured in all 8 mice. Cronbach's alpha was then calculated to assess reproducibility of repeat transillumination meibography measurements of meibomian gland area.

Results

As shown in Fig. 8, the structure of the meibomian glands in both the upper and lower eyelids of a young male mouse (2 month-old, # 1) were clearly visible using transillumination meibography (Supplemental Video 1). Acini appeared circular or elliptical and the central ducts of the glands were not apparent. In general, the proximal gland (orifices side) appeared narrow, while the distal region was wider. The meibomian glands appeared clearly separated from each other in the proximal region, while becoming less distinct in the distal regions. By scanning the eyelid with the light probe to the left and right, it was possible to observe seven meibomian glands in the upper eyelid. Since the temporal or nasal portion of the eyelids were not completely everted, meibomian glands in these areas were less distinct. Meibomian glands in the upper eyelids were 0.35–0.38 mm in width, 0.83–0.98 mm in length and contained acini of 0.05–0.08 mm in diameter (Table 1). The meibomian glands in the lower eyelid were similar though smaller than the upper lid (Fig. 8B, Video 2) ranging in size from 0.18 to 0.32 mm in width, 0.49–0.63 mm in length and contained acini of similar size, ranging from 0.05 to 0.08 mm in diameter (Table 1). In some of meibomian glands, a central transparent region could be identified between rows of acini (Fig. 8, C and C′) suggesting the presence of a central duct. In the lower eyelid, it was possible to observe 10 meibomian glands.

Young mice vs. old mice

The meibomian glands in the upper eyelid of the old mice appeared to show irregular shaped acini in three of the four mice suggesting Meibomian gland dropout (Fig. 9A asterisk, Video 3) (15 month old, mouse # 6). The meibomian glands in the lower eyelid appeared similar to the upper eyelids (Fig. 9B, Video 4). However, the measured size of the meibomian glands in the upper eyelids were similar to the meibomian glands in younger mice, ranging from 0.274 to 0.420 mm in width, 0.85–1.03 mm in length, and contained acini having 0.06–0.08 mm in diameter. Furthermore, the measured size of the meibomian glands in the lower eyelids also were similar to the meibomian glands in younger mice. Meibomian glands in the lower eyelids ranged from 0.25 to 0.30 mm in width, 0.56–0.72 mm in length and contained acini having 0.07–0.08 mm in diameter. The overall length of the meibomian glands was shorter than that of the upper eyelid.

As a quantitative comparison, the mean acinar area of the meibomian glands from young mice was 0.088 ± 0.025 mm^2 and 0.080 ± 0.020 mm^2 in old mice ($p = 0.564$), but the Meibomian gland density was significantly lower in old mice than in young mice (41.7 ± 6.4%, 27.3 ± 4.2%) ($p = 0.021$) (Table 2). Fig. 10 shows meibomian glands in the lower eyelids of young and old mice included in the study.

Author Manuscript Author Manuscript Author Manuscript Author Manuscript

Reproducibility of in vivo transillumination meibography

Mean acini area of a meibomian gland photographed on the first day was 0.084 ± 0.029 mm^2 and mean acini area of a meibomian gland photographed on the second day was 0.084 ± 0.031 mm^2 (Fig. 11). Cronbach's alpha was 0.905 (Fig. 12).

Among the 8 animals that underwent *in vivo* transillumination meibography, no mouse died due to the complications of anesthesia.

Discussions

In this study, *in vivo* transillumination meibography was performed on mice, which are animal models commonly used to study meibomian gland biology and pathobiology. As far as known, this is the first report that describes sequential, *in vivo* imaging of these glands to study changes in gland structure and function. Using mouse meibography, we confirm that the meibomian glands of old mice appear atrophic compared to those of the young mice. Specifically, acini shape appeared more irregular in older mice with some showing clear regions of acinar dropout unlike meibomian glands in younger mice. But, the mean acinar area of meibomian glands from younger mice were not significantly larger compared to older mice (0.088 ± 0.025 mm^2 and 0.080 ± 0.020 mm^2) ($p = 0.564$). Previous studies using 3D reconstruction of mouse meibomian glands and quantitative morphometry have shown significant loss of acini with age [14,16]. Our inability to detect a similar significant difference may be due, in part, to the small sample size and the 2-dimensional analysis of the meibographic images. Furthermore, we used image thresholding to objectively identify acinar area using ImageJ. While this approach removes operator bias in the outlining of acini, variation in tissue density and light scattering between old and young mice made it difficult to precisely segregate acini from non-acinar tissue in the older mice.

While it should be noted that Meibomian gland density was significantly lower in older mice than in young mice (41.7 ± 6.4%, 27.3 ± 4.2%) ($p = 0.021$), this reduced density may be also have been affected by the increased laxity of the eyelid in older mice that allowed for stretching of the eyelid. Nevertheless, repeat imaging of the meibomian glands showed that mouse meibography and objective, unbiased quantitative analysis of acinar area was highly repeatable over the short term. We therefore propose that application of this imaging system may provide novel insights into the effects of hormones, aging, stress and other risk factors on the development of MGD in various mouse models. More importantly, the effects of targeted meibomian gland therapies may more easily be assessed using this novel imaging approach.

That being said, mouse meibography has some difficulties. First, because the horizontal length of the eyelid is only 4 mm, eversion of the eyelid sufficient for high magnification photography is extremely difficult. Second, unlike human, mouse meibomian glands are not clearly visible in noncontact meibography of white mice such as BALB/c [30]. To overcome these drawbacks, our system used special forceps, special type of optical fiber, light probe including a prism, dissecting microscope, and transillumination.

Author Manuscript Author Manuscript Author Manuscript Author Manuscript

The most important parts of this system are the optical fibers, light probe and prism. The special optical fiber consists of 7 fibers arranged in a linear array to illuminate along the eyelid margin. The prism reflect the light 90° allowing light to pass through the meibomian glands vertically. In addition, when the eyelid margin was held with forceps, the prism helps to physically support the eyelid to aid photography. It is also important to note that the eyelids were everted by the double teeth forceps. These can symmetrically hold the eyelid margin during meibography, and help flatten the eyelid over the illuminating prism to avoid tissue distortion (Fig. 5). It should be noted that when the mouse eyelid was pulled over the prism only skin near the lid margin was pinched by the forceps. In this way, there is no direct injury to Meibomian glands (Fig. 11). In our repeat study, we were not able to detect any change in the structure of the meibomian gland on the second day, which would be important is repeat measures were used to evaluate the Meibomian gland before and after therapy or treatment.

In the present study, a monochromatic camera was used with no infrared blocking filter. In preliminary studies an infrared band pas filter that blocked visible and ultraviolet light was also used to image the meibomian gland. However, infrared transillumination images appeared no different from visible light images, which is consistent with our previous studies of light scattering from human and rabbit eyelid tissue.

In conclusion, this study is the first to report the successful *in vivo* transillumination meibography in mice, which are the most common animals of meibomian gland dysfunction animal models. Using this method, it was possible to effectively take photos of meibomian glands in large area of the upper and lower eyelids. This method can be used to evaluate the effects of certain treatments on meibomian gland dysfunction.

Supplementary Material

Refer to Web version on PubMed Central for supplementary material.

Acknowledgement

Financial Support: Supported by a grant from NIH/NEI EY021510 and a Research to Prevent Blindness Unrestricted Grant, a grant of the Korea Health Technology R&D Project through the Korea Health Industry Development Institute (KHIDI), funded by the Ministry of Health & Welfare, Republic of Korea (grant number: HI17C0659), Basic Science Research Program through the National Research Foundation of Korea (NRF) funded by the Ministry of Education, Republic of Korea(No. 2017R1A1A2A10000681) and Hallym University Research Fund (HURF-2017-59).

References

[1]. Craig JP, Nichols KK, Akpek EK, et al. TFOS DEWS II definition and classification report. Ocul Surf 2017;15:276–83. [PubMed: 28736335]

[2]. Bron AJ, de Paiva CS, Chauhan SK, et al. TFOS DEWS II pathophysiology report. Ocul Surf 2017;15:438–510. [PubMed: 28736340]

[3]. Knop E, Knop N, Millar T, et al. The international workshop on meibomian gland dysfunction: report of the subcommittee on anatomy, physiology, and pathophysiology of the meibomian gland. Invest Ophthalmol Vis Sci 2011;52:1938–78. [PubMed: 21450915]

Author Manuscript Author Manuscript Author Manuscript Author Manuscript

[7]. Corrales RM, Stern ME, De Paiva CS, et al. Desiccating stress stimulates expression of matrix metalloproteinases by the corneal epithelium. Invest Ophthalmol Vis Sci 2006;47:3293–302. [PubMed: 16877394]

[8]. De Paiva CS, Corrales RM, Villarreal AL, et al. Corticosteroid and doxycycline suppress MMP-9 and inflammatory cytokine expression, MAPK activation in the corneal epithelium in experimental dry eye. Exp Eye Res 2006;83:526–35. [PubMed: 16643899]

[9]. De Paiva CS, Yoon KC, Pangelinan SB, et al. Cleavage of functional IL-2 receptor alpha chain (CD25) from murine corneal and conjunctival epithelia by MMP-9. J Inflamm (Lond) 2009;6:31. [PubMed: 19878594]

[10]. Corrales RM, de Paiva CS, Li DQ, et al. Entrapment of conjunctival goblet cells by desiccation-induced cornification. Invest Ophthalmol Vis Sci 2011;52:3492–9. [PubMed: 21421863]

[11]. Coursey TG, Tukler Henriksson J, Barbosa FL, et al. Interferon-gamma-Induced unfolded protein response in conjunctival goblet cells as a cause of mucin deficiency in sjogren syndrome. Am J Pathol 2016;186:1547–58. [PubMed: 27085137]

[12]. Suhalim JL, Parfitt GJ, Xie Y, et al. Effect of desiccating stress on mouse meibomian gland function. Ocul Surf 2014;12:59–68. [PubMed: 24439047]

[13]. Tong L, Gupta PK. Need for animal models of meibomian gland dysfunction. Ophthalmol Ther 2016;5:129–34. [PubMed: 27837409]

[14]. Nien CJ, Paugh JR, Massei S, et al. Age-related changes in the meibomian gland. Exp Eye Res 2009;89:1021–7. [PubMed: 19733559]

[15]. Nien CJ, Massei S, Lin G, et al. Effects of age and dysfunction on human meibomian glands. Arch Ophthalmol 2011;129:462–9. [PubMed: 21482872]

[16]. Parfitt GJ, Xie Y, Geyfman M, et al. Absence of ductal hyper-keratinization in mouse age-related meibomian gland dysfunction (ARMGD). Aging (Albany NY) 2013;5:825–34. [PubMed: 24259272]

[17]. Mizoguchi S, Iwanishi H, Kokado M, et al. Ocular surface alkali injury damages meibomian glands in mice. Ocul Surf 2017;15:713–22. [PubMed: 28442381]

[18]. Chen Z, Huang J, Liu Y, et al. FGF signaling activates a Sox9-Sox10 pathway for the formation and branching morphogenesis of mouse ocular glands. Development 2014;141:2691–701. [PubMed: 24924191]

[19]. Dong F, Liu CY, Yuan Y, et al. Perturbed meibomian gland and tarsal plate morphogenesis by excess TGFalpha in eyelid stroma. Dev Biol 2015;406:147–57. [PubMed: 26363126]

[20]. Tsau C, Ito M, Gromova A, et al. Barx2 and Fgf10 regulate ocular glands branching morphogenesis by controlling extracellular matrix remodeling. Development 2011;138:3307–17. [PubMed: 21750040]

[21]. Jester JV, Rife L, Nii D, et al. In vivo biomicroscopy and photography of meibomian glands in a rabbit model of meibomian gland dysfunction. Invest Ophthalmol Vis Sci 1982;22:660–7. [PubMed: 7076409]

[22]. Robin JB, Jester JV, Nobe J, et al. In vivo transillumination biomicroscopy and photography of meibomian gland dysfunction. A clinical study. Ophthalmology 1985;92:1423–6. [PubMed: 4069605]

[23]. Mathers WD, Daley T, Verdick R. Video imaging of the meibomian gland. Arch Ophthalmol 1994;112:448–9.

[24]. Yokoi N, Komuro A, Yamada H, et al. A newly developed video-meibography system featuring a newly designed probe. Jpn J Ophthalmol 2007;51:53–6. [PubMed: 17295142]

[25]. Arita R, Itoh K, Inoue K, et al. Noncontact infrared meibography to document age-related changes of the meibomian glands in a normal population. Ophthalmology 2008;115:911–5. [PubMed: 18452765]

[26]. Pult H, Riede-Pult BH. Non-contact meibography: keep it simple but effective. Contact Lens Anterior Eye 2012;35:77–80. [PubMed: 21885325]

[27]. Srinivasan S, Menzies K, Sorbara L, et al. Infrared imaging of meibomian gland structure using a novel keratograph. Optom Vis Sci 2012;89:788–94. [PubMed: 22525129]

[28]. Arita R, Itoh K, Maeda S, et al. A newly developed noninvasive and mobile pen-shaped meibography system. Cornea 2013;32:242–7. [PubMed: 22580439]

Author Manuscript Author Manuscript Author Manuscript Author Manuscript

[29]. Eom Y, Han JY, Kang B, et al. Meibomian glands and ocular surface changes after closure of meibomian gland orifices in rabbits. Cornea 2018;37:218–26. [PubMed: 29189289]

[30]. Hyun Kyu L, lt Md, et al. Meibography and immunohistochemistric structures in animal models. J Korean Ophthalmol Soc 2018;59:9–16.

Author Manuscript Author Manuscript Author Manuscript Author Manuscript

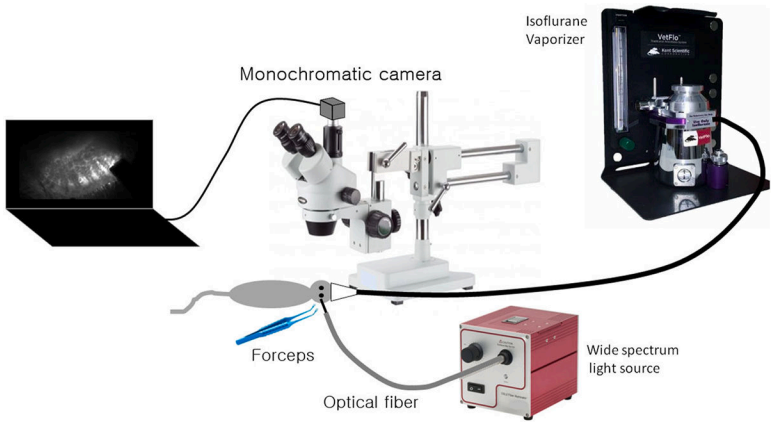

Fig. 1.

Overview of the *in vivo* meibography system for mice. This system was composed of a binocular dissection microscope (Leica MZ16FA, Leica Microsystems, Heerbrugg, Switzerland) equipped with a monochromatic camera (DFC340FX, Leica Microsystems, Heerbrugg, Switzerland), mouse holder, a halogen lamp (OSL2 and OSL2B, Thorlabs, Newton, NJ), optical fiber and light probe, forceps, inhalation and anesthesia system.

Author Manuscript Author Manuscript Author Manuscript Author Manuscript

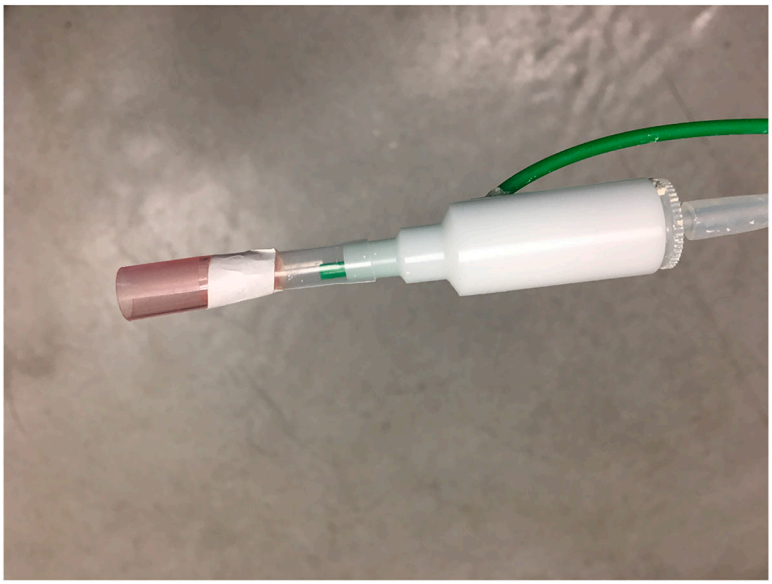

Fig. 2.

Inhalation mask for mice made with Ependorf tube and an anesthetic coaxial gas tube. Anesthesia was maintained using a customized inhalation mask (isoflurane 1.5–2.0%, 100 ml/min oxygen) fabricated using a 1 ml Eppendorf pipette tip connected to the anesthetic coaxial gas tube (Kent Scientific, Torrington, CT).

Author Manuscript Author Manuscript Author Manuscript Author Manuscript

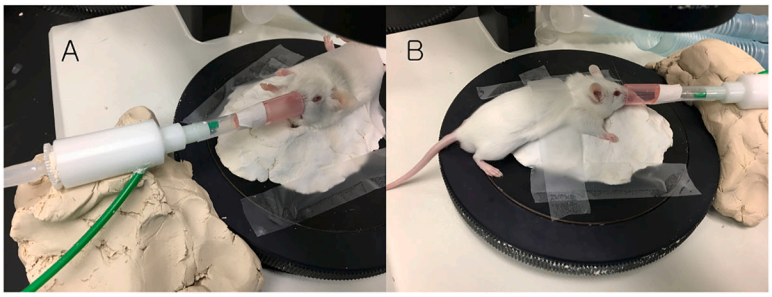

Fig. 3.

Mouse position and mouse holder. Because the mouse position is very important for good meibography, we used a mouse holder made with clay. The mouse was positioned so that the eyelids to be examined were located on the lower side. For example, when the meibomian glands in the upper lid were photographed, the mouse was placed in a supine position with the head adjusted so that the upper eyelid margin was horizontal (A), and the palpebral conjunctival plane was parallel to the objective lens of the dissecting microscope. For the lower eyelid, the mouse is placed in a prone position (B).

Author Manuscript Author Manuscript Author Manuscript Author Manuscript

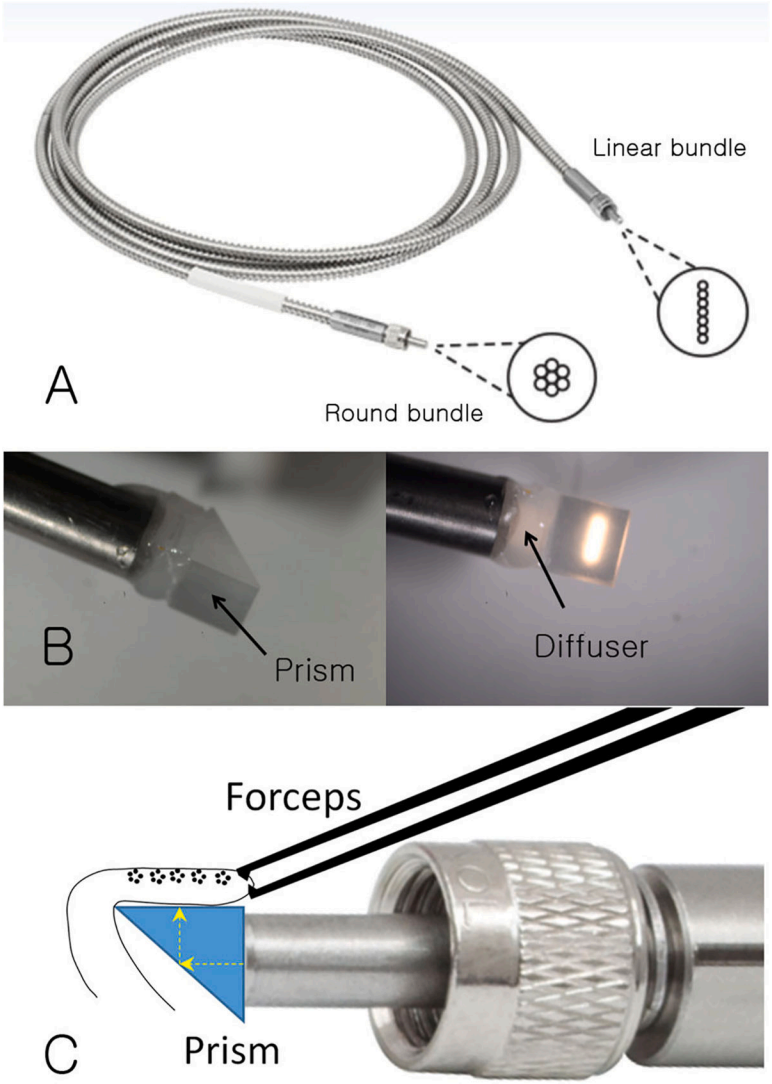

Fig. 4.

Optical fiber and light probe. The light was delivered by a special optical fiber (BFL200HS02, Thorlabs, Newton, NJ) that had an input connector comprised of a bundle of seven 200 μm-diameter fibers and an output connector comprised of a linear array of fibers (A). The linear array, output connector was then attached to a diffuser and a prism with glue. The diffuser was made of opaque, white plastic, 3 mm × 3 mm × 1 mm thickness. At the opposite end of the diffuser, a right-angle prism (PS605, Thorlabs, Newton, NJ) (3 mm) was attached (B) that reflected the light 90° to pass through the meibomian glands vertically. In addition, when the eyelid margin was held with forceps, the prism served to support the eyelid at the back (C).

Author Manuscript Author Manuscript Author Manuscript Author Manuscript

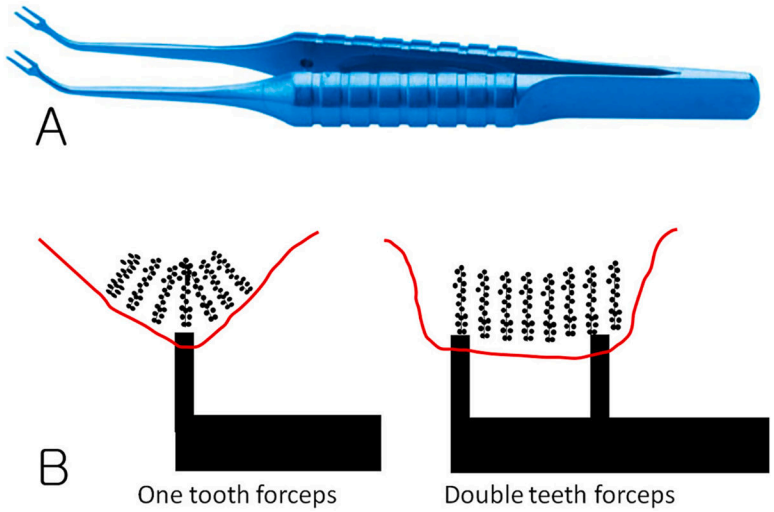

Fig. 5.

Polack forceps for eyelid eversion. Polack forceps (8–0814T, Rumex, Clearwater, FL) was used to evert the eyelids (A). Polack forceps are special type of forceps used in cornea transplantation surgery. They have two pairs of teeth that can symmetrically hold the edges of a corneal button during corneal suturing. When the lid margin of mouse was held with these forceps and everted, the eyelid was flat and was not distorted to a triangular shape (B).

Author Manuscript Author Manuscript Author Manuscript Author Manuscript

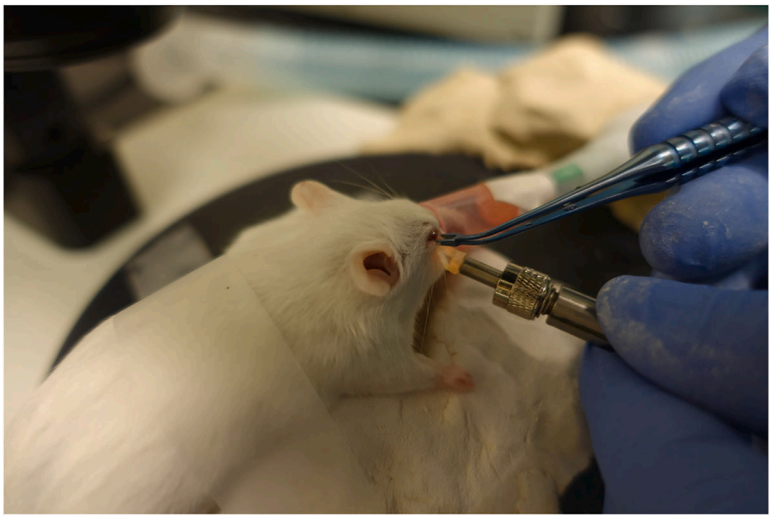

Fig. 6.

Taking photographs. First, at a low magnification, the position of the mouse was adjusted so that the eyelid to be examined was located at the center of the field of view. The magnification was then increased to 28.3X, maintaining focus on the lid margin. Using the Polack forceps the middle edge of the eyelid margin was grasped, and eyelid pulled over the prism to evert the eyelid. The meibomian glands were then brought into focus by adjusting the height of the light probe and the forceps holding the eyelid.

Author Manuscript Author Manuscript Author Manuscript Author Manuscript

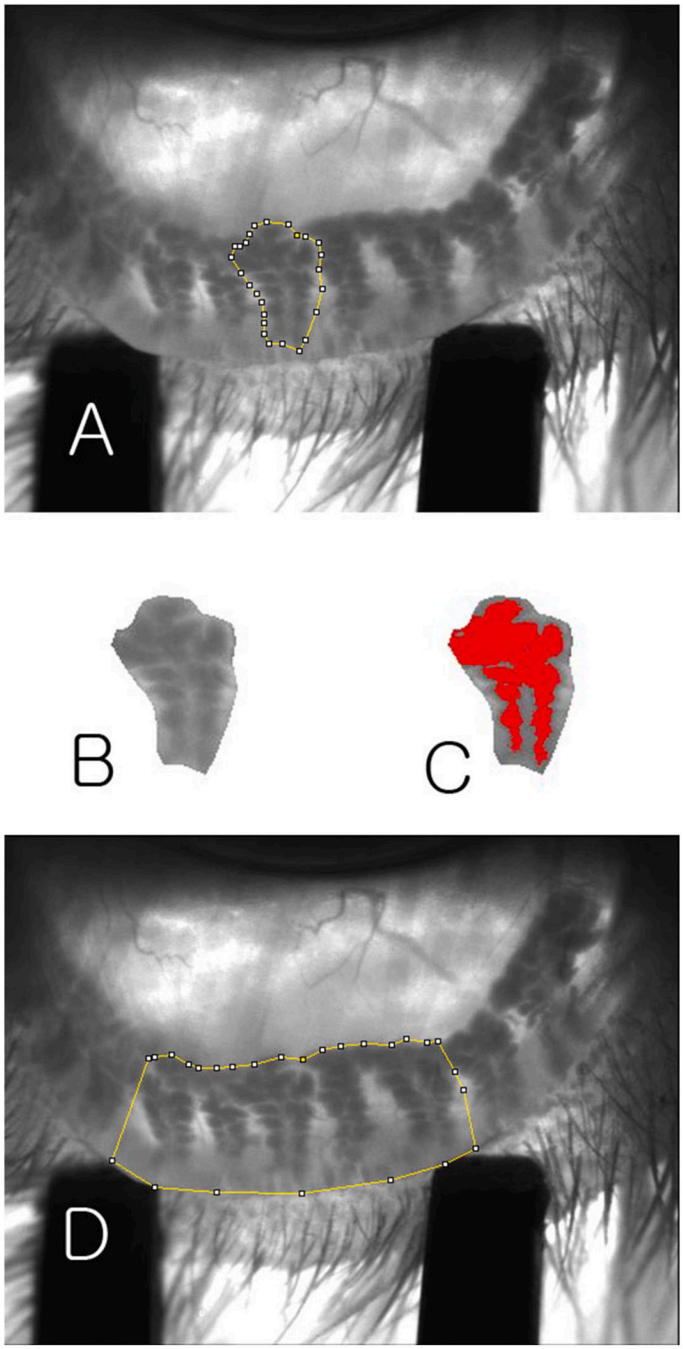

Fig. 7.

Methods for quantitative analysis. For each image, each Meibomian gland was then selected (A, B) using image J (version 1.38x; Wayne Rasband National Institutes of Health, Bethesda, MD) and the image threshold was adjusted so that only the acini were selected (C). The area occupied by the acini was then recorded. Acinar area was measured for each of five meibomian glands (MG_1, MG_2, MG_3, MG_4, MG_5), as well as the total acinar areas for the five meibomian glands ($MG = MG_1+MG_2+MG_3+MG_4+MG_5$) and mean acini area of a meibomian gland (MG/5). For each image, a region of interest (ROI) was defined

Author Manuscript Author Manuscript Author Manuscript Author Manuscript

by outlining five meibomian glands like Fig. 7D (from eyelid margin to distal end of Meibomian glands). The area of the region of interest covering the five meibomian glands (ROIA) was then measured and the Meibomian gland density was calculated 100% * total acinar area of five meibomian glands (MG)/total area of region of interest covering the five meibomian area (ROIA).

Author Manuscript Author Manuscript Author Manuscript Author Manuscript

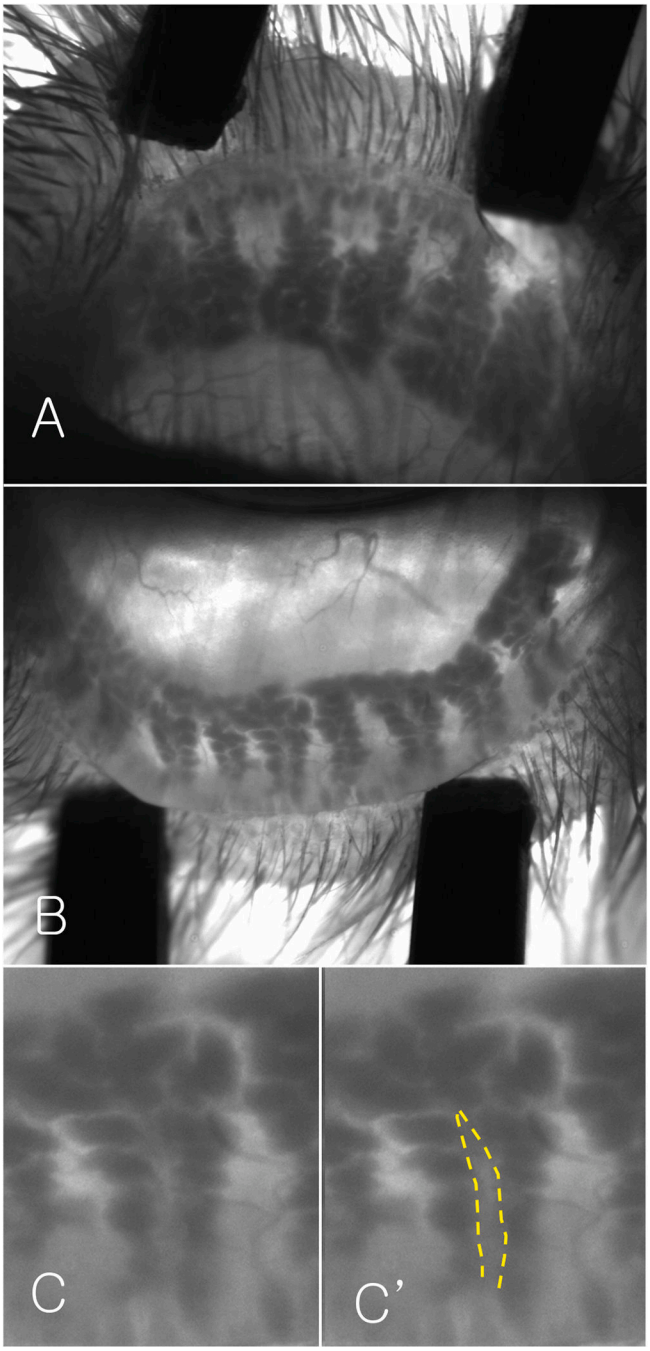

Fig. 8.

The meibomian glands in the upper and lower eyelid of a young male mouse The structure of the meibomian glands in both the upper (A) and lower (B) eyelids of a young male mouse (2 month-old, # 1) were clearly visible using transillumination meibography. Acini appeared circular or elliptical and the central ducts of the glands not apparent. In general, proximal gland (orifices side) appeared narrow, while the distal region was wider. The meibomian glands appeared clearly separated from each other in the proximal region, while becoming less distinct in the distal regions. In some of meibomian glands, a central transparent region

Author Manuscript Author Manuscript Author Manuscript Author Manuscript

could be identified between rows of acini (C) suggesting the presence of a central duct which is outlined in C'.

Author Manuscript Author Manuscript Author Manuscript Author Manuscript

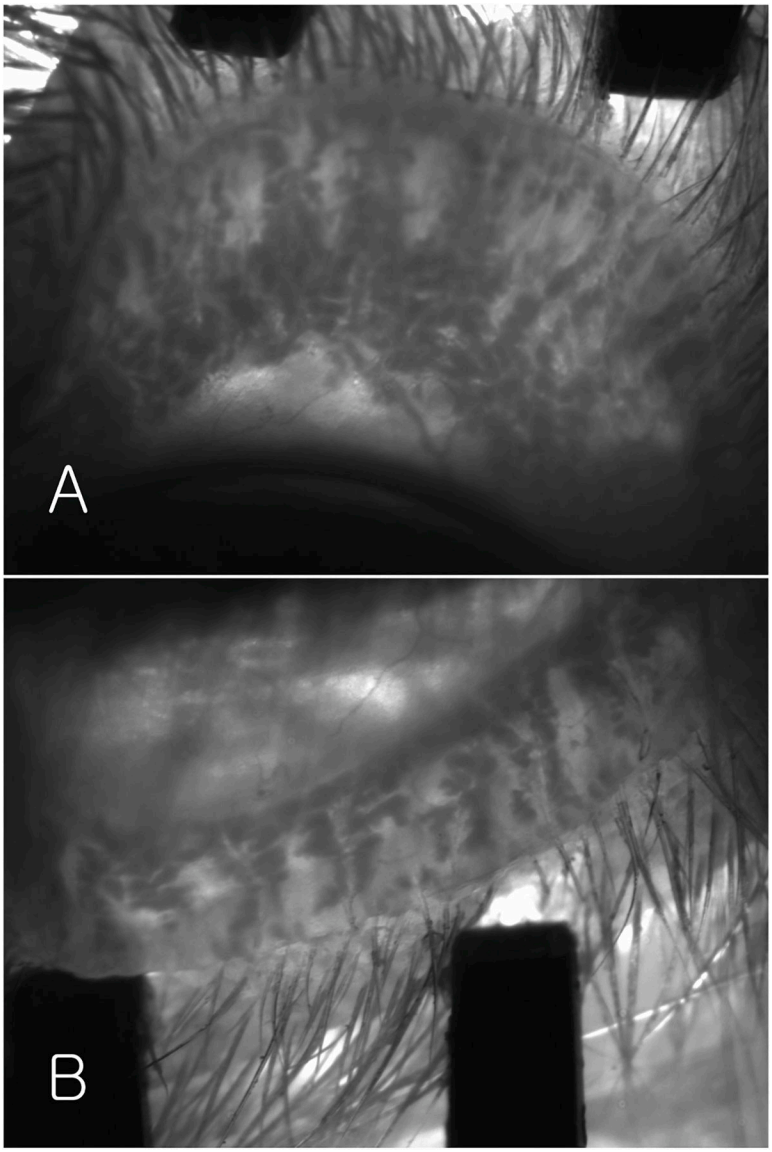

Fig. 9.

The meibomian glands in the upper and lower eyelid of an old male mouse. The meibomian glands in the upper eyelid of the old mice (15 month old, mouse # 6) showed irregular shape acini and apparent dropout (A). The meibomian glands in the lower eyelid appeared similar to in the upper eyelids (B). The overall length of the meibomian glands was shorter than that of the upper eyelid.

Author Manuscript Author Manuscript Author Manuscript Author Manuscript

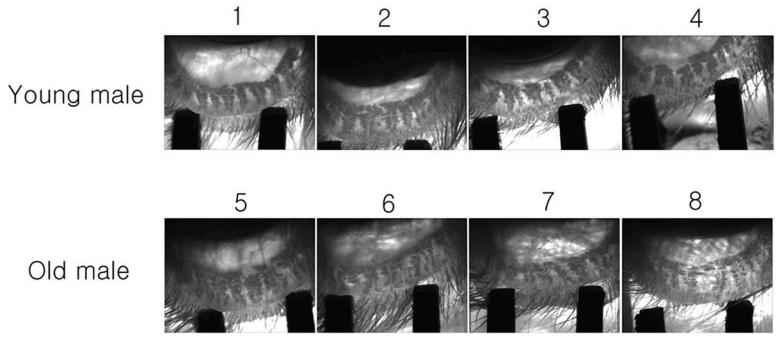

Fig. 10.

The meibomian glands in the lower eyelid of young and old male mice. The meibomian glands in the lower eyelid of the young mice showed circular or elliptical acini no dropout. But, the meibomian glands in the lower eyelid of the old mice showed irregular shape acini and apparent dropout.

Author Manuscript Author Manuscript Author Manuscript Author Manuscript

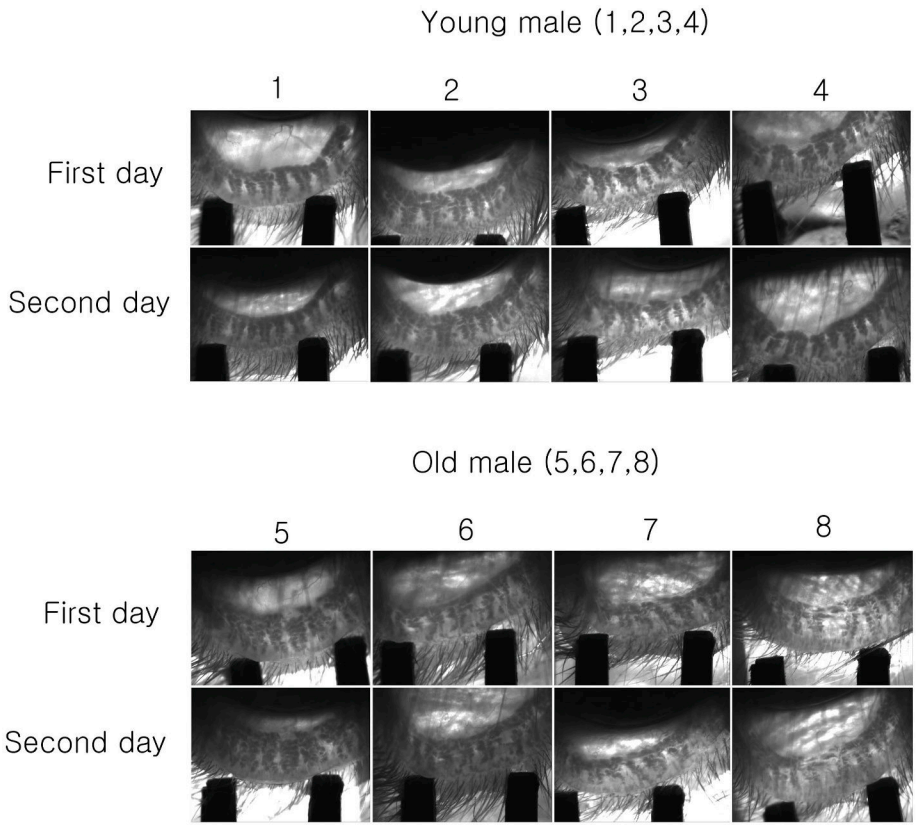

Fig. 11.

In vivo transillumination meibography taken first day and second day. The meibomian glands in the lower eyelid taken first day appeared very similar to those taken second day.

Author Manuscript Author Manuscript Author Manuscript Author Manuscript

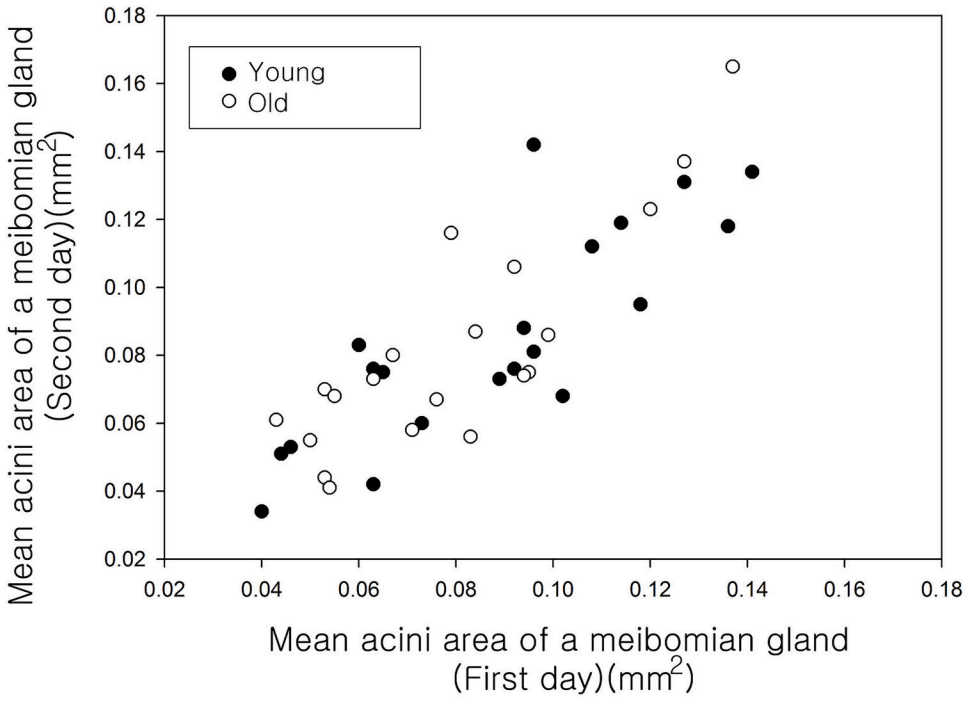

Fig. 12.

Reproducibility of *in vivo* transillumination meibography. Mean acini area of one meibomian gland photographed on the first day was 0.084 ± 0.029 mm^2 and mean acini area of a meibomian gland photographed on the second day was 0.084 ± 0.031 mm^2. Cronbach's alpha was 0.905.

Author Manuscript

Author Manuscript

Author Manuscript

Author Manuscript

Table 1

Width, length and acinus diameter of meibomian glands in the upper and lower eyelids of young and old male mice.

	Young male mice (n = 4)	Old male mice (n = 4)
Meibomain glands in the upper eyelids	**n = 20**	**n = 20**
Width (mm)	0.35–0.38	0.27–0.42
Length (mm)	0.83–0.98	0.85–1.03
Acinus diameter (mm)	0.05–0.08	0.06–0.08
Meibomain glands in the lower eyelids	n = 20	n = 20
Width (mm)	0.18–0.32	0.25–0.30
Length (mm)	0.49–0.63	0.56–0.72
Acinus diameter (mm)	0.05–0.08	0.07–0.08

Author Manuscript Author Manuscript Author Manuscript Author Manuscript

Ocul Surf. Author manuscript; available in PMC 2023 July 31.

Table 2

Quantitative analysis between meibomian glands of young male mice and old male mice.

	Young male mice						Old male mice						
	Mouse #1	**Mouse #2**	**Mouse #3**	**Mouse #4**	**Mean**	**SD**	**Mouse #5**	**Mouse #6**	**Mouse #7**	**Mouse #8**	**Mean**	**SD**	**P-value**
MG_1 (mm^2)	0.089	0.118	0.114	0.063			0.079	0.053	0.053	0.050			
MG_2 (mm^2)	0.063	0.141	0.044	0.046			0.092	0.071	0.043	0.063			
MG_3 (mm^2)	0.092	0.127	0.096	0.060			0.099	0.095	0.054	0.083			
MG_4 (mm^2)	0.073	0.096	0.040	0.065			0.127	0.055	0.076	0.094			
MG_5(mm^2)	0.102	0.136	0.108	0.094			0.137	0.067	0.084	0.120			
Mean acini area per MG (mm^2)	0.084	0.124	0.080	0.066	**0.088**	**0.025**	0.107	0.068	0.062	0.082	**0.080**	**0.020**	**0.564** [a]
Total acini area of five MGs (mm^2)	0.420	0.618	0.402	0.328	**0.442**	**0.124**	0.536	0.342	0.311	0.411	**0.400**	**0.100**	**0.564** [a]
Area of ROI covering the five meibomian area (mm^2)	0.906	1.318	0.999	0.985	**1.052**	**0.182**	1.611	1.293	1.197	1.756	**1.464**	**0.263**	**0.083** [a]
Meibomian gland density (%)	46.4	46.9	40.2	33.3	**41.7**	**6.4**	33.3	26.4	26.0	23.4	**27.3**	**4.2**	**0.021** [a]

SD: Standard deviation.

MG: Meibomian gland.

ROI: Region of interest.

[a]Mann-Whitney u-test.